

Rotor Slot Distance Effects on Output Parameters in Single Phase Induction Motors

Merve Şen Kurt¹  and Ahmet Fenercioğlu²

¹Amasya University, Department of Electric and Electronic Engineering, Amasya, TURKEY.

²Gaziosmanpaşa University, Department of Mechatronic Engineering,, Tokat, TURKEY

ABSTRACT

In this paper, single phase induction motor which has different rotor slot distances are analyzed with 2-D Finite Element Method (FEM). The analyses are carried out using ANSYS/Maxwell program which solves equations with FEM. The model has same stator and rotor slot geometry. The variable parameter is slot distance which is between outer diameter of rotor core and top border of slot. The single phase induction motor model has 2 poles, 96 W shaft power and run capacitor. It is connected to 220 V, 50 Hz AC network under the full load. Slot distance is varied from 0.2 to 1 mm in 0.1 mm steps. Magnetic model is solved for each distance. Electrical performance characteristics which are speed, efficiency, current, torque and power factor (PF) are determined. Magnetical flux density (B), flux lines and current density on bars are demonstrated visually. Motor performance is improved as the slot distance decrease.

Keywords:

Efficiency, Design and optimization, Single phase induction motor, Finite element method, Rotor slot distance

Article History:

Received: 2017/06/23

Accepted: 2017/09/30

Online: 2018/03/28

Correspondence to: Merve Sen Kurt,
Amasya University, Department of Electric
and Electronics Engineerin, Amasya,
TURKEY.

Tel: +90 (358) 260-0066 (1468)

E-Mail: mervesenkurt@gmail.comcoils,

INTRODUCTION

Single phase induction motors (SPIMs) nowadays are widely used in domestic and commercial areas because of cheap cost, simple structure, low noise and small dimensions etc. Split phase, start and run-capacitor single phase induction motors are well known SPIM motor types [1]. Although a lot of advantages have mentioned, a SPIM has some disadvantages. Its efficiency is low and starting performance is not so good to compare the other electrical machines types.

The optimal design of an induction motor in terms of electromagnetic torque means starting and breakdown torques are higher value [2]. Many researchers have investigated to improve the starting torque and efficiency of a SPIM. Some of them have focused the influence of rotor slot geometry like rotor slot type, shape, skewing, number of rotor slot, slot opening and core material.

Zhou Rui et al [3], have modeled two single phase induction motors with Maxwell 2D software and changed their dimensions in Maxwell 2D to find optimal slot geometry with respect to starting performance and efficiency. In similar studies; S. Sobhani et al [4] have examined dimensions of two SPIMs and mechanical

shaft torque, rated slip, efficiency and power factor are compared. Literature [5,6] have investigated air gap flux densities for pear-shaped, circular and trapezoidal slots. They have simulated and analyzed with FEM. The literature [7] presents the advantage of double cage rotor over the single cage rotor induction motor. The literature [8] investigated the effect of rotor slots opening on torque and efficiency on SPIM. It was concluded that torque is destroyed around the slot opening because of the the rotating magnetic field. Optimal stator slot opening and closing have minimal effect of negative torque [8]. In the literature, effects of rotor slot shapes which are pear, trapezoidal and rounded shaped on harmonics of airgap flux densities were investigated and reported 1st, 3th, 5th, 27th and 29th harmonics [9]. Literature show that rotor slot geometry has an incredible effect in the motor performance. In this paper, rotor slot distance influences on SPIM with run capacitors have been examined. Speed, currents, shaft torque, power factor, efficiency have predicted and compared by 2D FEM for each slot distance.

MATHEMATICAL APPROXIMATIONS

The motor performance is affected by the parameters of rotor resistance and rotor leakage reactance in a squirrel cage induction motor. Rotor slot leakage flux

depends on rotor slot geometry, saturation of magnetic material, rotor frequency and current density in the rotor.

Rotor bar inductance is derived from magnetic co-energy is calculated by using Eq. 1 [10].

$$W_m = \frac{1}{2} \iiint \vec{B} \cdot \vec{H} \cdot dV = \frac{1}{2} i^2 L \quad (1)$$

Ampere's law is applied by using Eq. 2. Where l is the length of bar, B is the magnetic flux density (T), I is bar current and μ_0 is permeability of vacuum [10].

$$\oint \vec{B} \cdot d\vec{l} = \mu_0 I \quad (2)$$

Bar inductance is calculated from Eq. 3

$$L_b = \frac{1}{2i^2} \mu_0 I \int_0^{h_{s2}+r} H^2(h) \cdot b(h) \cdot dh \quad (3)$$

Where, h_{s2} is rotor bar depth, dh is variable of bar depth,

Table 1. The rotor slot dimensions of the SPIM

Symbol	Quantity	Size
hs_2	The depth of rotor slot	4 mm
bs_1	The upper width of rotor slot	3.67 mm
bs_2	The lower width of rotor slot	2.96 mm
bs_0	The edge width of rotor slot	1 mm
hs_0	The distance of rotor slot from rotor core	0.2 – 1 mm
A	Slot area	21.856 mm ²
r_1	Radius of slot top circle	1.835 mm
r_2	Radius of slot bottom circle	1.48 mm

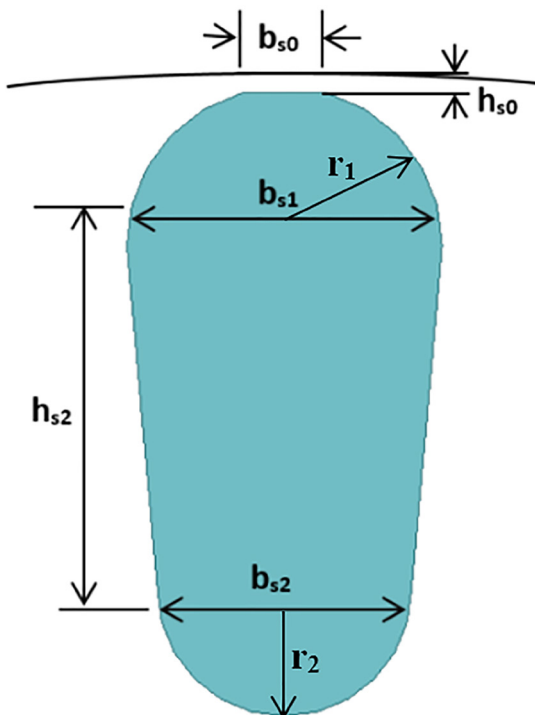


Figure 1. The geometry of drip-shaped rotor slot.

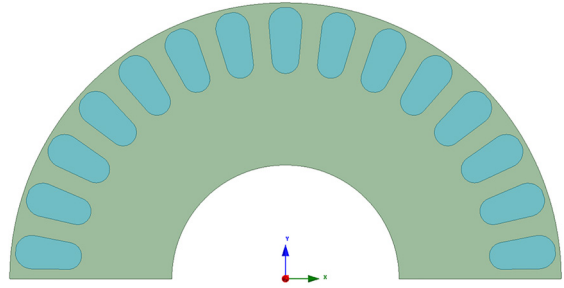


Figure 2. The cross section of rotor half model

r is total radius of bar circles (r_1+r_2). The inductance of rotor bar is depend on magnetic permeability coefficient (λ) by using Eq. 4 [10].

$$L_b = \mu_0 I \cdot N^2 \cdot \lambda \quad (4)$$

Magnetic permeability coefficient (λ) differs according to rotor slot types. The literature [11-13] have presented detailed calculations for different rotor slot types. In this study, designed model has drip-shaped rotor slot. Fig. 1 shows the geometry of drip-shaped rotor slot, Table 1 shows the dimensions of the SPIM.

The coefficient λ is calculated by using Eq. 5 [10]. Where k_2 parameter is defined a value 0.645 to 0.785, the inductance attenuation factor, k_1 is a value less than 1.

$$\lambda = \frac{hs_2}{3 \cdot bs_1} k_1 + k_2 - \frac{hs_0}{2 \cdot bs_1} + \frac{hs_0}{bs_0} \quad (5)$$

METHODS OF ANALYSIS

2D analyses of motor and external circuits for excitations were carried out using ANSYS/Maxwell FEA software and symmetrical half model was analyzed in transient and steady state conditions under full load which is 0.31 Nm load torque. Analysis sampling frequency is 18 Khz, analysis period is 1 second and starting speed is 0, rated speed is about 2950 rpm.

Model of the SPIM

Model SPIM has squirrel-cage rotor, 96 W shaft power, 2950 rpm speed, 0.31 Nm load torque. It is connected 220 V, 50 Hz AC network. Fig. 2 shows the rotor cross section. Main and auxiliary windings are placed in 24 slots of the stator magnetic core. Rotor and stator cores made of laminated steel material with 0.95 stacking factor to reduce eddy current losses on its periphery.

As shown in Fig.2 the rotor has 30 slots which are drip-shaped and parallel tooth. The squirrel cage rotor consists of cast aluminium bars with bulk conductivity is 23×10^6 S and relative magnetic permeability is 1.000021.

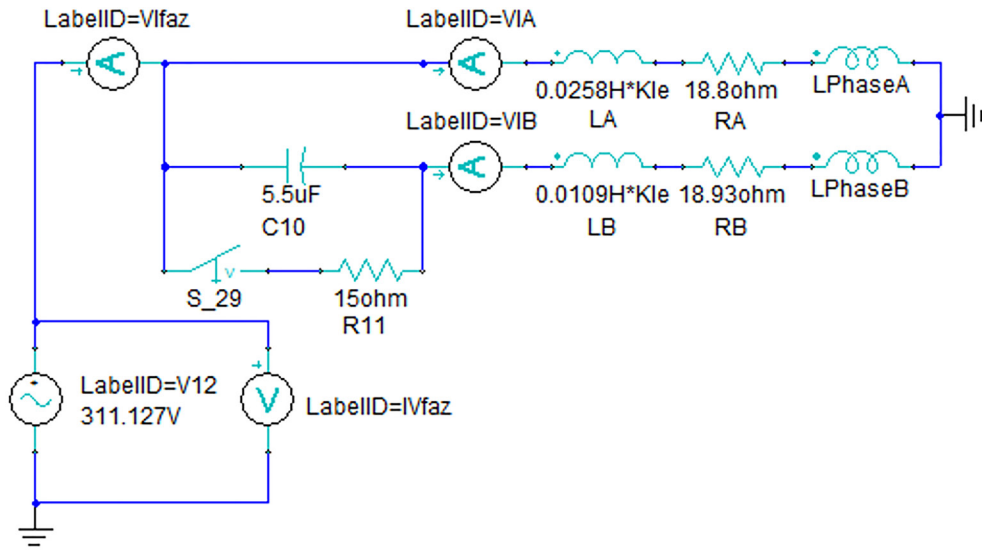


Figure 3. External circuit of the SPIM

External Electric Circuit

The major problem which is a single-phase network does not produce a rotating magnetic field. Instead, the magnetic field produced by a single-phase source remains stationary in position and pulses with time. Since there is no net rotating magnetic field, conventional induction motors cannot function, and special designs are necessary [14]. So, the single phase motor needs an auxiliary winding which produces phase angle and rotating magnetic field. The external circuit of the model is given in Fig. 3.

Each horizontal branch represents main and auxiliary windings. R_A' , L_A' , L_{phaseA} , R_B' , L_B' and L_{phaseB} are respectively main winding resistance, end winding inductance, phase inductance, auxiliary windings resistance, end winding inductance and phase inductance. Phase inductances depend on magnetic flux. Run capacitor is serial connected to auxiliary winding, starting resistor is parallel connected to run capacitor. Starting resistor is switched off after starting.

FINITE ELEMENT ANALYSIS (FEA)

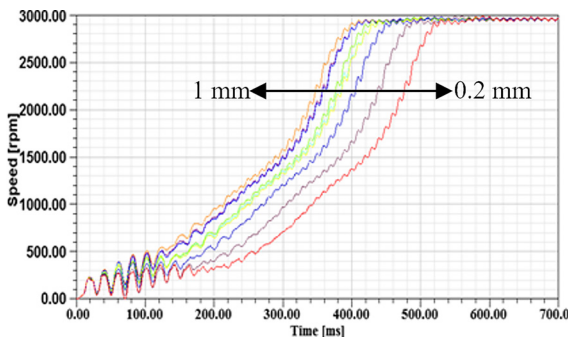


Figure 4. Acceleration and transient time

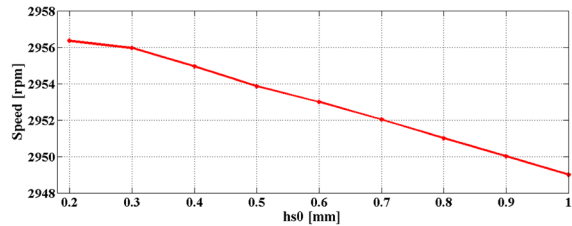


Figure 5. Rated speed versus to rotor slot distance

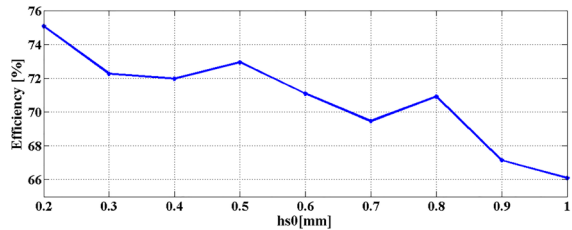


Figure 6. Efficiency versus to rotor slot distance

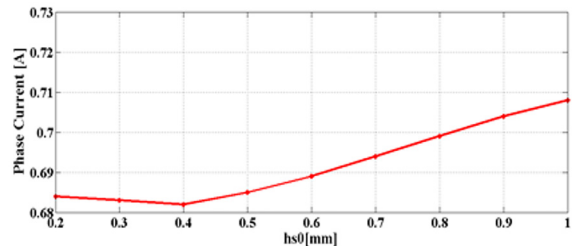


Figure 7. Phase current versus to rotor slot distance

2D transient analyses of motor were carried out by using FEA method. The calculations were obtained from different rotor slot distances ($hs0$) from 0.2 to 1 mm in 0.1 mm steps. Fig. 4 shows the change in speeds for transient and steady states. The smaller slot distance is the longer starting time. Fig. 5 shows changing in average value of speed according to the rotor slot distance for steady-state condition. As it can be seen in Fig. 4, the motor reaches

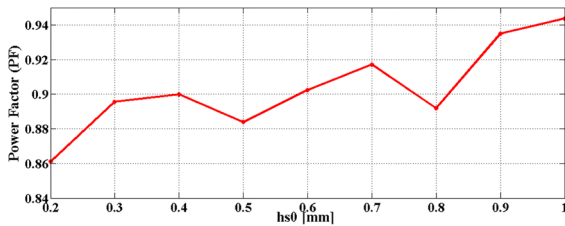


Figure 8. Power factor versus to rotor slot distance from the core

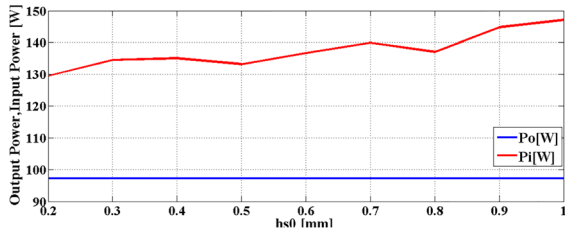


Figure 9. Output power according to rotor slot distance

steady state after 600 ms and average speed values are very close for all of the rotor slot distances. As the distance increases 0.2 to 1 mm in 0.1 mm steps, motor speed decreases because of changes the inductance of rotor bar (Eq. 4 and Eq.5).

Fig. 6 shows that the rotor slot distance increases from 0.2 to 1 in 0.1 mm steps. When it was reach to 1 mm, the efficiency was decreased by 11,96%.

The phase current which is the sum of the main

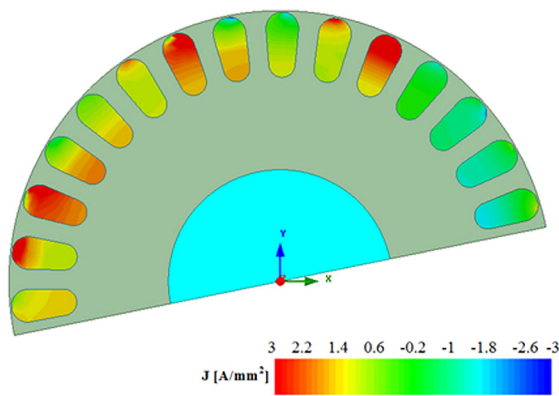


Figure 10. Current density distribution on rotor slots

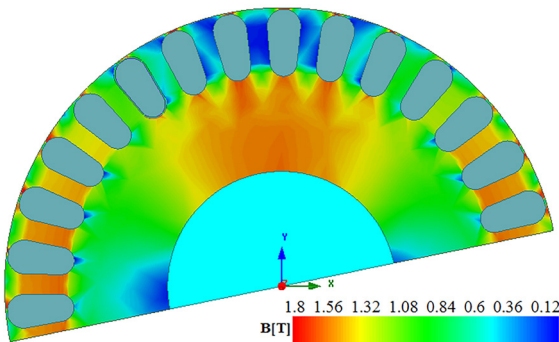


Figure 11. The distribution of the magnetic field density on stator and rotor cores

Table 2. Limit values of flux density [16,17]

Position B_g	Flux Density[16]	Maximum Flux Density[17]
Airgap,	0,65-0,82 T	
Stator yoke	1,1-1,45 T	1,7 T
Stator teeth	1,4-1,7 T	2,1 T
Rotor yoke	1,2 T	1,7 T
Rotor teeth	1,5-1,8 T	2,2 T

and auxiliary windings currents is shown in Fig. 7. The maximum value of phase current is calculated as 0.71 A in 1 mm slot distance.

The power factor varies according to rotor slot distance is shown in Fig. 8 It is depended on magnetic flux in air gap. Magnetic flux density varies according to flux path length. The longer slot distance is increase flux path and leakage reactance. For this reason power factor is rised. The output torque is constant for each slot distance. It is shown in Fig. 9.

Bar current density and core magnetic flux density have to take into consideration besides electrical performance variables when an optimal slot geometry is chosen. Current density (J) on the rotor bars have to be in range $2,2 < J < 4,5$ A/mm² for small motors with alemnium rotor bars [15]. Bar current density distributions on rotor slots have been shown in Fig. 10.

Magnetic flux densities in air gap, stator yoke, stator teeth, rotor yoke and rotor teeth have to be in range of Table 2 which shows the permitted limit values in the literature. Fig. 11 shows the distribution of the magnetic field density on stator and rotor cores.

As can be seen in Fig. 11 maximum values of flux density is 1.118 T in rotor yoke, 1.577 T in rotor teeth, 1.224 T in stator yoke and 1.186 T in stator teeth, respectively. It can be concluded that rotor yoke and rotor teeth, stator yoke and stator teeth don't exceed permitted limit values in Table 2.

Table 3. Rotor slot distances effects on performance

Parameters	Slot distance (0.2 mm)	Slot distance (1 mm)
Transient time	420 ms	540 ms
Rated speed	2956 rpm	2949 rpm
Phase current	0.684 A	0.708 A
Electromagnetic Torque	0.337	0.339
Load torque	0.314	0.315
Power Factor	0.86	0.94
Input Power	129.510	147.076
Output power	97.223	97.209
Efficiency	75.070	66.094

CONCLUSION

This study investigates the impact of rotor slot distance on the electrical performance of single phase induction motor. Rotor slot distance is between rotor core outer diameter and top border of rotor slot. The distance is increased from 0.2 mm to 1 mm in 0.1 mm steps. Motor performance is determined for each distance. The longer slot distance, the motor starting time is shorter, the rated speed and the efficiency are lower. As the slot distance is increased, the phase current, the electromagnetic torque and the power factor are increased. Performance values are given in Table 3 for 0.2 mm and 1 mm slot distances. The λ coefficient in Eq. 4 and Eq. 5 depends on slot distance (h_{so}). If the rotor slot distance is smaller, motor electrical performance is improved. 0.2 mm slot distance is the optimal solution in this study.

ACKNOWLEDGEMENT

This paper is presented in ICAT'17 at Istanbul Conference, and published in proceeding book as abstract. It is supported by 2016/81 numbered Gaziosmanpasa University BAP Project.

References

1. Mademlis C, Kioskeridis I, Theodoulidis T. Optimization of single-phase induction motors-part I: maximum energy efficiency control. *IEEE Transactions on Energy Conversion* 20(1), (2005) 187-195.
2. Fireteanu V, Tudorache T, Turcanu OA. Optimal design of rotor slot geometry of squirrel-cage type induction motors, 2007 In. Conf. on Electric Machines & Drives, Antalya, Turkey, 2007, pp. 537-542.
3. Rui Z, Qunjing W, Guoli L, Guanghui F. Optimal design of single-phase induction motor based on maxwell 2D rmxprt. 15th Int. Conf. on Electrical Machines and Systems, Incheon, South Korea, 2010.
4. Sobhani S, Yaghobi H, Samakoosh M. Optimize efficiency and torque in the single-phase induction motor by adjusting the design parameters. 12th Int. Conf. on Environment and Electrical Engineering, Wroclaw, Poland, 2013.
5. Zhang K, Jiang X, Wu Y, Zhang L, Wu X. Effect of slot shape in rotor of electrical motor with high-speed spindle on slot ripples. 2nd Int. Conf. on Modelling, Identification and Control (ICMIC), Okayama, Japan, 2010, pp. 670-675.
6. Turcanu OA, Tudorache T, Fireteanu V. Influence of squirrel-cage bar cross-section geometry on induction motor performances. 23rd Int. Conf. on Power Electronics, Electrical Drives, Automation and Motion (SPEEDAM), Taormina, Italy, 2006, pp. 9-15.
7. Yahaya Enesi, Omokhafa T, Agbachi EO, James AG. Advantage of double cage rotor over single cage rotor induction motor, *Innovative Systems Design and Engineering*, 6 (12), (2015) 1-4.
8. Jang GH, Park SJ. Characterization of a single-phase induction motor due to the effect of slot opening, *IEEE Transactions on Magnetics*, 40 (4), (2004) 2065-2067.
9. Negoita A, Scutaru G, Peter I. Influence of rotor static eccentricity on the noise level of a single phase squirrel cage induction motor, 13th International Conference on Optimization of Electrical and Electronic Equipment (OPTIM), Brasov, Romania, 2012, pp. 373-378.
10. Şal S, İmeryüz M, Ergene L. Kafesli asenkron motorlarda maliyet kısıtı altında rotor çubuklarının analizi, *EMO Bilimsel Dergi*, 2(3), (2012) 23-28.
11. Boldea I, Nasar SA. *The Induction Machine Handbook*, second ed. CRC Press, New York, 2002.
12. Pyrhönen J, Jokinen T. *Design of Rotating Electric Machines*, second ed. Wiley Press, New Delhi, 2008.
13. Gürdal O. *Elektrik Makinalarının Tasarımı*, first ed. Nobel Press, İstanbul, 2006.
14. Chapman SJ. *Elektrik Machinery Fundamentals*, fourth ed. McGraw-Hill, New York, 2005.
15. Fu F, Tang X. *Induction Machine Design Handbook*, China Machine Press, Beijing, 2001.
16. Say MG. *Performance and Design of AC Machines*, third ed. Pitman Publishing, London, 1970.
17. Lipo TA. *Introduction to AC machine Design*, third ed. Wiley-IEEE Press, Madison, 2004.